ELSEVIER

Journal of Molecular Catalysis A: Chemical 125 (1997) 53–62

JOURNAL OF MOLECULAR CATALYSIS A: CHEMICAL

Oxidative dehydrogenation of 1-butene over Zn–Al ferrites

J.A. Toledo [a,b,*], P. Bosch [b], M.A. Valenzuela [c], A. Montoya [a], N. Nava [a]

[a] *Instituto Mexicano del Petróleo, STI. Gcia. de Catalizadores, Lázaro Cárdenas # 152, A.P. 14-805, 07730 México D.F., México*

[b] *Universidad Autónoma Metropolitana-Iztapalapa, Depto. Química, Av. Michoacán y la Purísima, A.P. 55-532, 09000 México D.F., México*

[c] *Instituto Politécnico Nacional, ESIQIE, UPALM-Zacatenco, 07738 México D.F., México*

Received 1 July 1996; accepted 25 February 1997

Abstract

The aluminum introduction into the zinc ferrite $ZnFe_{2-x}Al_xO_4$ in the range $0.0 \leq x \leq 1.0$ was studied. These ferrites were calcined at two temperatures, 550°C and 750°C. X-ray diffraction (XRD) patterns showed that they have a spinel structure with Al^{3+} replacing Fe^{3+} in octahedral sites. The crystallite size decreased as the aluminum introduction increased. At high calcination temperature, sintering and segregation processes occur. Linear correlations were found between XRD and Mössbauer parameters. Mössbauer spectra showed that the symmetry of the electron distribution decreased around the nucleus of Fe^{3+}, as the aluminum content increased. Such asymmetrical distribution of the electron density may be associated to the spatial accommodation of aluminum in the neighboring octahedral sites. Oxygen atoms turn out to be more basic due to the charge transfer from Fe^{3+} to O^{2-} in the Fe–O bond. Hence the acid–base type dissociation of the C–H bond for the *n*-butenes activation is favored. The highest yield of butadiene was obtained for the samples treated at 750°C whereas for the samples calcined at 550°C, double bond isomerization of 1-butene occurs in competition with the oxidative dehydrogenation. © 1997 Elsevier Science B.V.

Keywords: Aluminum zinc ferrite; X-ray diffraction; Mössbauer spectroscopy; 1-butene oxidative dehydrogenation; Metal oxides; Spinels; Ferrites

1. Introduction

The addition of foreign cations of different valence states can lead to a variety of tetrahedral and octahedral site coordinations in solid solution. These changes in site occupation and cation valence states are associated with valence induction in the crystal resulting from foreign-ion addition. Such modifications have been of special interest in the control of the electronic properties of spinels [1,2].

Iron oxide is a well known heterogeneous catalyst, mainly for oxidation processes [3]. In the oxidative dehydrogenation of hydrocarbons, a solid solution of α-Fe_2O_3 and metals such as Zn, Mg, Ni, etc. is used [4]. If iron is substituted by chromium in the octahedral sites of the spinel structure of ferrites, the electronic properties and, thus, the catalytic activity in the oxidative dehydrogenation of 1-butene [5] and *n*-butane [6] are modified. Recently we have reported a strong variation in the electronic properties by the introduction of a low amount of iron in the zinc aluminate spinel structure [7].

* Corresponding author.

PII S1381-1169(97)00052-6

The selectivity to butadiene in the oxidative dehydrogenation of 1-butene on iron oxide has been reported to depend on the specific surface area of the catalysts [8], on their crystallite size [9], on the metal–oxygen bond strength in their structure [3], and on the crystallographic structure. For instance, the spinel γ-Fe_2O_3, has been found to be more selective to butadiene than α-Fe_2O_3 which presents a corundum lattice [10].

In all spinels only the (111) and (110) planes constitute the surface [11]. Hence, only octahedrally coordinated cations are exposed to the reactants [12]. In our previous work [7] we found that if a small amount of iron is introduced into the $ZnAl_2O_4$ network by impregnation or coprecipitation method, the catalytic activity and the butadiene selectivity in oxidative dehydrogenation of 1-butene are improved. In this work we study the effect of aluminum introduction into the zinc ferrite. Aluminum may, indeed, substitute iron atoms in the octahedral sites of the spinel and it is virtually inactive in the oxidative dehydrogenation of 1-butene which is the chosen test reaction. Therefore, we examine the dilution effect of aluminum on the iron active sites and the corresponding modifications of the oxidative dehydrogenation of 1-butene to butadiene. We have chosen to test our catalysts with the oxidative dehydrogenation of 1-butene instead of that of *n*-butane (of more practical importance) because oxidative dehydrogenation of paraffins may be performed in homogeneous phase without catalysts [13,14]. The thermal activity, in paraffins, may mask the catalytic activity.

2. Experimental

2.1. Catalyst preparation

$ZnFe_{2-x}Al_xO_4$ catalysts were synthesized by coprecipitation from an aqueous solution of the corresponding nitrates. The precipitation was carried out with an aqueous solution of NH_4OH (50%) at 50°C and constant pH (7.5) adding simultaneously NH_4OH and the nitrate solution. The obtained gels were carefully washed with distilled water, filtered and dried at 110°C overnight in a vacuum oven. Two fractions of this material were calcined in air flow for 6 h at 550°C and 750°C respectively. The two series of samples thus obtained were labeled as C*m*–*n* where C means 'coprecipitation', *m* the calcination temperature and *n* the nominal substitution degree of Fe^{3+} by Al^{3+}, i.e., *x* value in

Table 1
Nominal composition, surface area, crystallite size and lattice parameter of Zn–Fe–Al mixed oxides

Catalysts	*x* in $ZnFe_{2-x}Al_xO_4$	XRD surface area [a] (m^2/g)	BET surface area (m^2/g)	Crystallite size [b] (Å)	Lattice parameter (Å)
C550-0.00	0.00	39	18	291	8.441
C550-0.10	0.10	47	35	238	8.424
C550-0.25	0.25	64	37	177	8.396
C550-0.50	0.50	73	50	154	8.350
C550-0.75	0.75	110	69	102	8.315
C550-1.00	1.00	127	66	89	8.271
C750-0.00	0.00	< 20	1	> 600	8.442
C750-0.10	0.10	< 20	1	> 600	8.424
C750-0.25	0.25	< 20	1	> 600	8.392
C750-0.50	0.50	< 20	1	> 600	8.333
C750-0.75	0.75	61	10	184	8.285
C750-1.00	1.00	60	12	188	8.248

[a] These were calculated from the average crystallite size by assuming spherical crystallites.
[b] Average crystallite size determined by the line broadening of X-ray diffraction.

$ZnFe_{2-x}Al_xO_4$. The nominal compositions are presented in Table 1.

2.2. X-ray diffraction (XRD)

X-ray diffraction patterns were obtained with a Siemens D500 diffractometer equipped with a copper anode X-ray tube and a diffracted beam monochromator (K α radiation). Crystallite size was measured from the broadening of the (311) diffraction peak, applying the Debye–Scherrer equation [15]. To be sure that the morphology of the crystallite did not determine the crystallite size, the Debye–Scherrer equation was applied to all peaks present in the C550-0.0 diffractogram. In all cases, similar crystallite size values were obtained, hence only the (311) spinel diffraction peak was used for the other samples. An error of ± 10 Å was determined. Cell parameters were calculated, using the (311) reflection plane of silicon (NBS-640B, JCPDS-27-1402) as an internal standard [16]. The error was determined to be ± 0.005 Å.

2.3. Mössbauer spectroscopy

Mössbauer spectra of the two series of catalysts were collected with a conventional constant acceleration spectrometer Austin Scientific Associates S-600, equipped with a krypton proportional detector. The γ-radiation source was ^{57}Co in a rhodium matrix (25 mCi). Velocity calibration was performed with a laser ray beam using an iron foil as reference. A standard least-squares minimization routine was used to fit the spectra as a superposition of Lorentzian lines. The spectra were obtained at room temperature. The source velocity was varied in the range ± 2 mm s^{-1} with a constant acceleration. All Mössbauer parameters are relative to α-Fe, and the accuracy was found to be ± 0.01 mm s^{-1}.

2.4. BET surface areas

BET surface areas of all samples were obtained by nitrogen physisorption in a Micromeritics ASAP-2000 apparatus.

2.5. Catalytic activity

Catalytic activity in the oxidative dehydrogenation of 1-butene was evaluated using a conventional continuous flow system at atmospheric pressure. The reactor was fed with a mixture of 5 mol% of 1-butene (Matheson C.P), 5 mol% of oxygen (Linde 99.6% purity) and 90 mol% of helium (Linde 99.6% purity). The total flow rate was 60 cm^3 min^{-1} and 0.2 g of catalyst was used for each test. Before reaction test, each fresh sample was heated at the reaction temperature (420°C) and pretreated under air flow (30 cm^3 min^{-1} for 1.5 h), in order to start with surfaces free of impurities and totally oxidized. The reaction products were analyzed in an on-line Varian Aerograph 3700 gas chromatograph equipped with a 30 ft (23% SP-1700 on 80/100 Chromosorb P AW) column and a thermal conductivity detector (TCD). Activities and yields were measured for one hour on stream. The intrinsic activities were calculated using the BET surface area results. The error on catalytic conversion and yield was ± 3. The yields were calculated as the moles of the interesting products (butadiene, CO_2, *cis*- and *trans*-2-butenes) divided by the total amount (in moles) of 1-butene in the feed.

3. Results and discussion

3.1. X-ray diffraction

The most representative X-ray diffraction patterns of the first series of catalysts, (samples calcined at 550°C) are presented in Fig. 1; they show the characteristic peaks of the spinel structure $ZnFe_2O_4$ (JCPDS 22-1012). The background line is flat showing that the amount of amorphous material, if any, is not significant. The diffraction peaks are broad and their broadening increases with aluminum content. In the samples C550-0.75 and C550-1.0, (i.e. in those with the highest aluminum content), small amounts of α-Fe_2O_3 (JCPDS 24-72) and ZnO (JCPDS 5-0664) were observed.

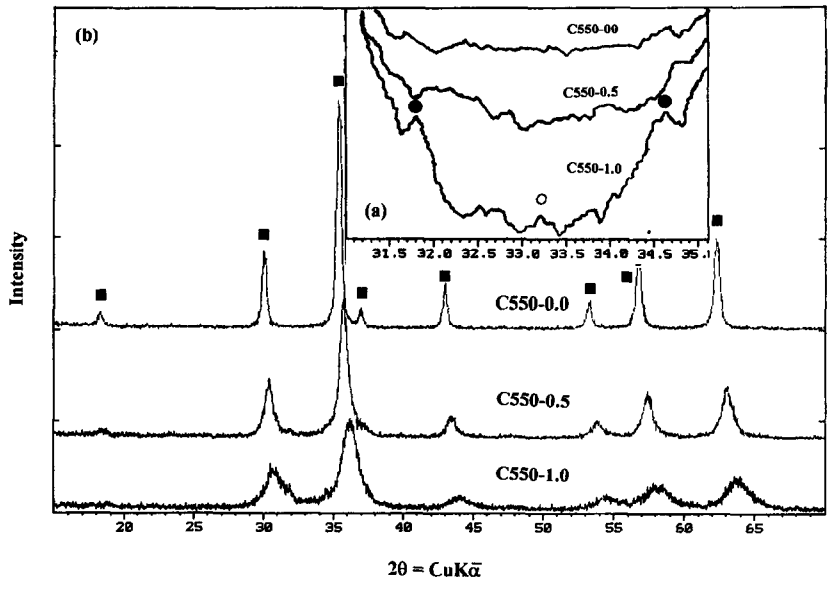

Fig. 1. X-ray diffraction patterns of catalysts calcined at 550°C. ■ $ZnFe_2O_4$; ○ α-Fe_2O_3; ● ZnO. (a) $30 \leq 2\theta \leq 35$. (b) Total diffractogram.

The most representative diffractograms of the second series of catalysts (samples calcined at 750°C) are presented in Fig. 2. In this case the samples are more crystalline. The peaks are sharper and the background line is totally flat. They show $ZnFe_2O_4$ as the main compound. In the catalysts C750-0.0 and C750-0.1, α-Fe_2O_3 is segregated. Although the samples C750-0.25 and C750-0.5 do not present any segregated phase they may be present in small amounts as

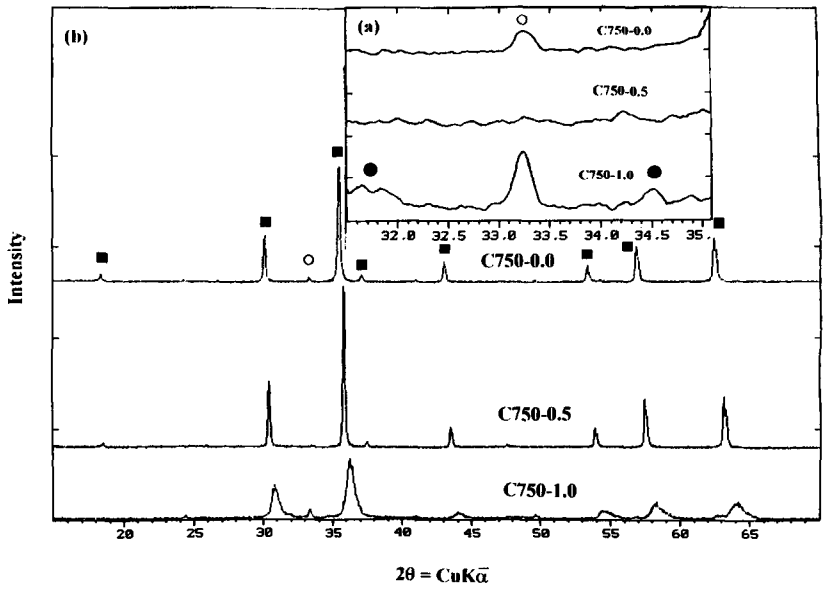

Fig. 2. X-ray diffraction patterns of catalysts calcined at 750°C. ■ $ZnFe_2O_4$; ○ α-Fe_2O_3; ● ZnO. (a) $30 \leq 2\theta \leq 35$. (b) Total diffractogram.

X-ray diffraction patterns are sensitive only to ca. 4% of crystalline compounds; if the compounds are microcrystalline or amorphous they are not observed. In samples C750-0.75 and C750-1.0, both α-Fe_2O_3 and ZnO are observed. The composition of these catalysts differs significantly from the catalysts reported in our previous work [7], as in that case segregated compounds were not observed. This behavior can be attributed to the difference in elemental composition. If the Fe or Al contents are low, these atoms may be easily located in the network, whereas if the Fe and Al contents are high, as in this work, they are expected to diffuse out of the network with temperature. Furthermore iron in a alumina spinel network should be less mobile than aluminum in an iron oxide spinel as the atomic radii are different ($r(Al^{3+}) = 0.50$ Å and $r(Fe^{3+}) = 0.64$ Å) [17].

Crystallite sizes were measured for catalysts of both series and are reported in Table 1. In samples calcined at 550°C, crystallite size decreases with the isomorphic substitution of iron by aluminum. For catalysts calcined at 750°C, the largest crystallites were found in C750-0.0, C750-0.10, C750-0.25 and C750-0.5 samples. Surprisingly for the catalysts C750-0.75 and C750-1.0, whose aluminum content was the highest, crystallite size decreased down to less than 200 Å. Surface areas were estimated from the crystallite size data assuming that crystallites were spherical; these values will be compared later with the BET results. However a clear difference is already established between C550 and C750 catalysts.

Lattice parameters are reported in Table 1 and plotted against aluminum content in Fig. 3. In both series of catalysts lattice parameter decreases with the aluminum content. Al^{3+} has an ionic radius (0.50 Å) smaller than Fe^{3+} (0.64 Å) [17]. It seems, therefore, that Fe^{3+} is substituted by Al^{3+} in the spinel network. Furthermore, C550 catalysts do not significantly deviate from the prediction by Végard's law [16], which was obtained from two extreme values: $ZnFe_2O_4$ and $ZnAl_2O_4$ reported in JCPDS cards.

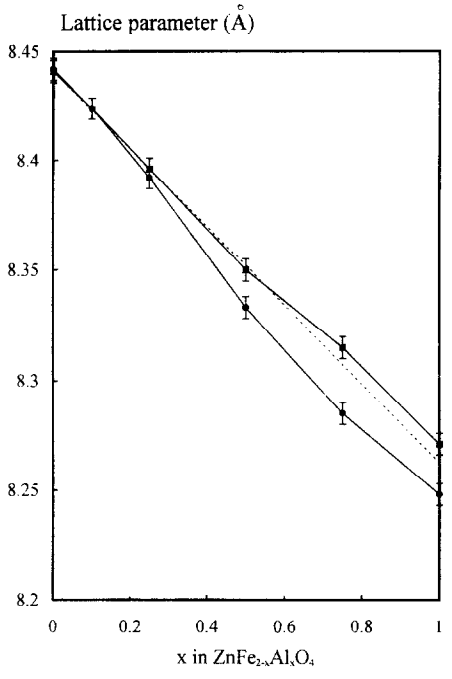

Fig. 3. Lattice parameters of C550 (– ■ –) and C750 (– ● –) catalysts. The Végard law prediction is presented (- - -).

In contrast, the C750 catalysts show a clear negative deviation from Végard's law. These results can be discussed considering the segregation of α-Fe_2O_3. If the spinel was iron enriched the deviation would be positive. As it is aluminum enriched the deviation is negative. Hence no alumina-like phases are expected as all aluminum is probably incorporated into the spinel structure. Furthermore, the phases α-Fe_2O_3 and ZnO are observed, the composition of the spinel phase is richer in Al and the real aluminum content x value is higher than the nominal amount in the spinel structure. Therefore, in samples calcined at 550°C a more homogeneous distribution of aluminum in the octahedral sites of the spinel structure is found than in C750 catalysts.

3.2. BET surface area

In order to verify if any amorphous microporous phase was segregated, BET surface areas were measured. These phases should contribute to an enhancement of the background line in

X-ray diffraction patterns, but, if their amount is low it is difficult to determine it. BET surface areas increase with aluminum content in both series of catalysts from values 18–69 and 1–12.

As the BET surface area is systematically lower (ca. 40%) than the surface area determined from crystallite size, two models can be proposed. The zinc ferrite crystallites could be occluded into an alumina particle. The second one would be a particle constituted by agglomerated small crystallites, or twinned crystals. In the first possibility alumina is a microporous material and the corresponding surface area would be large. Furthermore, the amount of Al_2O_3, if any, is too small. Hence, this model has to be discarded, and complex particles constituted by several $ZnFe_{2-x}Al_xO_4$ crystallites are expected.

3.3. Mössbauer spectroscopy

Mössbauer spectra of all samples were obtained at room temperature, Fig. 4. Both series

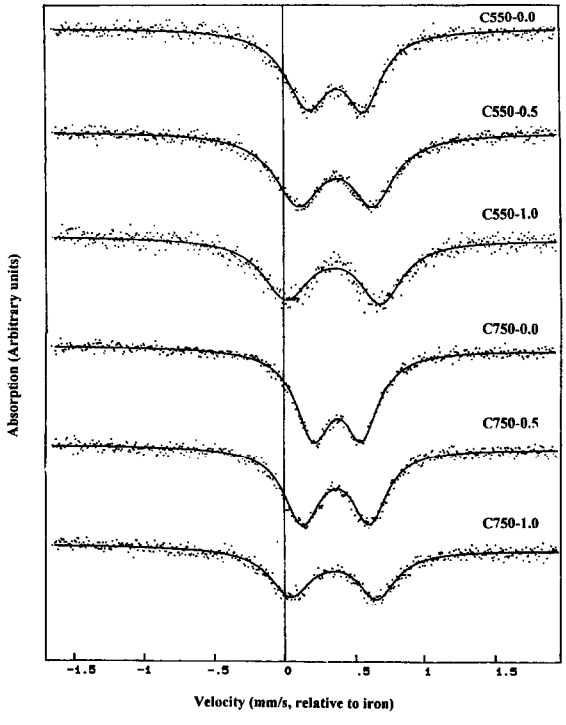

Fig. 4. Mössbauer spectra of C550 and C750 catalysts, obtained at 2 mm/s velocity and room temperature.

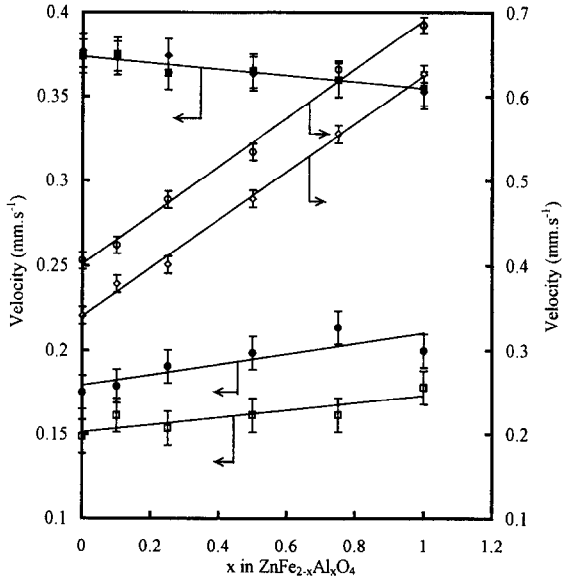

Fig. 5. Mössbauer parameters of C550 and C750 catalysts, relative to natural iron. I.S. C750 (– ◆ –), I.S. C550 (– ■ –), H.LW. C750 (– □ –), H.LW. C550 (– ● –), Q.S. C750 (– ◇ –), Q.S. C550 (– ○ –).

of spectra present a doublet close to zero velocity, which may be attributed to Fe^{3+} located in the octahedral sites of the spinel structure [18]. As aluminum content increases, in both C550 and C750 catalysts, the double peak does not shift considerably (isomer shift), although the interval between the peaks increases (quadrupole splitting). No evidence of any split magnetic peaks characteristic of α-Fe_2O_3 was observed, probably due to the iron superparamagnetic peaks overlapping ($ZnFe_{2-x}Al_xO_4$ and α-Fe_2O_3).

Mössbauer parameters calculated from the fitted spectra are presented in Fig. 5. All parameters show a linear dependance on the substitution degree of Fe^{3+} by Al^{3+} in the spinel structure. The isomer shift (I.S.) values are all characteristic of Fe^{3+} in octahedral environment in the whole range of aluminum concentration. They did not vary with calcination temperature but decreased as aluminum content increased, therefore s-electron density at the nucleus of the Fe^{3+} seems to increase.

The quadrupole splitting (Q.S.) parameter, also presented in Fig. 5, shows a linear increase

with x value (substitution degree of Fe^{3+} by Al^{3+} in the octahedral sites of the spinel structure). This result agrees with the XRD and the BET measurements: no segregated phases of Al_2O_3 are present. All aluminum is incorporated into the spinel network. Hence, the symmetry of the electron distribution around the nucleus of Fe^{3+} decreases, a lattice distortion is, then, due to the isomorphic substitution of Fe^{3+} by Al^{3+} on the neighboring octahedral sites. Such distortion of the electric field gradient which causes high quadrupole splitting, seems to be associated with the spatial accommodation of the substituent Al^{3+} cations in the octahedral sites of the spinel structure [19]. In catalysts calcined at 550°C, within experimental error range (± 0.01 mm s^{-1}), Q.S. parameters are higher than in C750 catalysts (Fig. 5). To summarize, cations that are distributed homogeneously produce an asymmetry in the electric field gradient of the Fe^{3+} nuclei.

Half line-width (H.LW.) parameters are also presented in Fig. 5. H.LW. is nearly independent of x; however the value for $x = 0.0$ is higher for the 550°C treated catalysts and, hence, the lines are parallel. This increase in H.LW. may be attributed to a different bulk electronic environment of the resonant atom [20]. Hence, the concentration of surface atoms (Fe^{3+} content), which have a different electronic environment, will affect the Mössbauer parameters mainly in C550 catalysts.

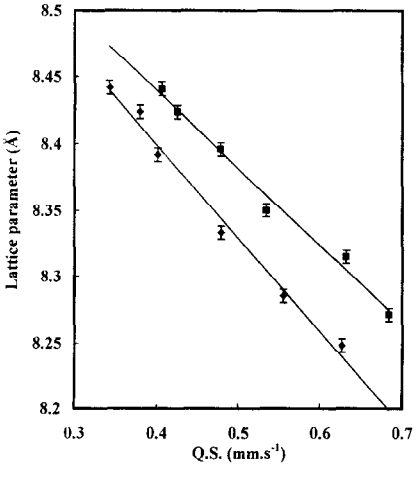

Fig. 6. Lattice parameters vs. quadrupole splitting of C550 (– ■ –) and C750 (– ◆ –) catalysts.

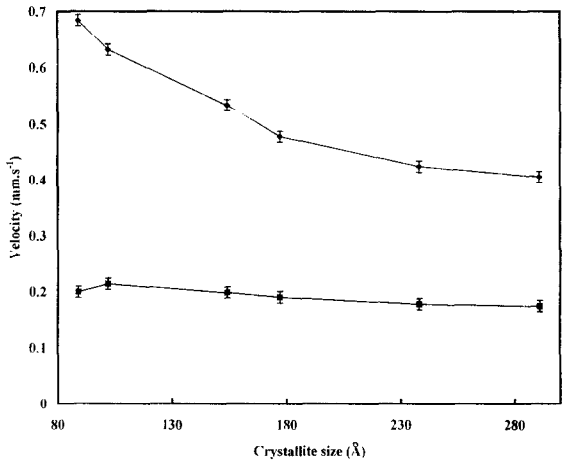

Fig. 7. Mössbauer parameters vs. crystallite size of C550 catalysts. Q.S. (– ◆ –) and H.LW. (– ■ –).

Fig. 6 is a plot of lattice parameter vs. Q.S. for catalysts calcined at 550°C and 750°C. A linear correlation is obtained, with a slope of -0.6 and -0.7 for C550 and C750 catalysts respectively. Hence, the increase in Q.S. parameter is clearly due to two phenomena that may give rise to an electric field gradient variation: the first one is the presence of aluminum atoms located in the iron positions surrounded by iron atoms. The second one is a deformation of the FeO_6 octahedra due to the presence of smaller cations in the structure.

However, if Mössbauer parameters are correlated to crystallite size determined by X-ray diffraction, Fig. 7, for the samples calcined at the same temperature (550°C), Mössbauer half line-width is independent of crystallite size within experimental error range, but Q.S. decreased as crystallite size increased. Therefore, Q.S. depends on lattice deformation and crystallite size [21,22].

3.4. Catalytic activity

The catalytic properties were studied as a function of the surface area by varying the calcination temperature and the aluminum con-

tent (Table 2). On the one hand, the conversion level was higher in samples calcined at 550°C than in samples calcined at 750°C. On the other hand, the intrinsic activity tends to decrease if x values in C550 or C750 catalysts increase. The highest yield of butadiene (36%) was reached with C750-0.75 catalyst, whereas the lowest butadiene yield was obtained with C750-0.25 sample. It seems that at low calcination temperature the butadiene yield (21 to 31%) is not very sensitive to x values. The CO_2 yield was not changed with aluminum content in C550 catalysts. However, in C750 catalysts the CO_2 yields were lower than those of C550 samples, Table 2, but tended to increase in the same way as butadiene yield increased. These results indicate that CO_2 comes from the combustion of butadiene or its precursor.

As Al and Zn are both virtually inactive in the oxidative dehydrogenation of hydrocarbons [23], the butadiene formation could be due to an Fe^{3+} active site which is the only reducible metal in the catalysts. In spite of that, the Al dilution effect on Fe sites was not observed, because the butadiene yield did not change dramatically compared with pure $ZnFe_2O_4$. These results could be attributed to the distortion of the electric field gradient at the Fe^{3+} nucleus (determined by our Mössbauer results). Therefore, there is a charge transfer from Fe^{3+} to O^{2-} in the Fe–O bond. Thus the oxygen bonded to Fe^{3+} and Al^{3+} atoms is more basic than the oxygen only bonded to Fe^{3+} in $ZnFe_2O_4$. Hence, the acid–base type dissociation of the C–H bond [24] for the butene activation to produce butadiene and CO_2 is favored. So the dilution effect is inhibited.

A competitive reaction in oxidative dehydrogenation of 1-butene is the double bond shift to produce *trans*- and *cis*-2-butenes. Double bond isomerization is favored by the catalysts treated at the lowest calcination temperature as well as by those with x values higher than 0.25 (Table 2). Hence an Al homogeneously distributed seems to be required. For catalysts calcined at the highest temperature the isomerization reactions are not significant because aluminum is not homogeneously incorporated into the spinel network as has been shown by the XRD results, Fig. 3.

The double bond isomerization of 1-butene is known to be an adequate reaction test to evaluate the acid and basic character of solids [25]. In solid acid catalysis a 2-butyl cation intermediate mechanism is followed while in solid base catalysis a π-allyl intermediate is followed.

Table 2
Activity and yield results on Zn–Fe–Al-mixed oxides

Catalysts	Conversion (mol %)	Intrinsic activity [a] $(\text{mol m}^{-2} \cdot \text{s}^{-1}) \times 10^7$	Yield (mol%)			*Cis*/*trans* ratio [b]
			butadiene	CO_2	2-butenes	
C550-0.00	50	1.76	21	11	18	1.26
C550-0.10	61	1.15	27	10	23	1.22
C550-0.25	66	1.18	26	10	30	1.02
C550-0.50	66	0.88	30	11	25	1.04
C550-0.75	69	0.69	31	10	27	1.00
C550-1.00	63	0.64	26	10	27	0.97
C750-0.00	14	6.08	10	2	2	1.42
C750-0.10	20	8.28	14	3	3	1.62
C750-0.25	5	2.51	3	1	1	1.28
C750-0.50	9	5.37	6	1	1	1.09
C750-0.75	49	3.27	31	9	9	1.46
C750-1.00	55	3.01	36	11	9	1.31

[a] These were calculated as number of 1-butene molecules reacted per m^2 of catalysts per second.
[b] These were calculated dividing *cis*-2-butene/*trans*-2-butene selectivity.

These two mechanisms yield different *cis*-2-butene/*trans*-2-butene ratios, i.e a *cis*/*trans* ratio lower than 1.0 indicates acid behavior but if it is higher than 3 it indicates base behavior. For 550°C treated catalysts, the *cis*-2-butene/*trans*-2-butene ratio, Table 2, decreases as the x value increases, showing that Al introduction in the spinel structure network increases the sample acidity.

When the samples are calcined at 750°C, the intrinsic activity improved, showing that the surface structure of those catalysts contains more iron active sites (segregated phase Fe_2O_3 on the spinel) than the surface structure of the C550 samples. Although the 750°C treated samples contain a spinel with a high aluminum content the *cis*/*trans* values do not correspond to an acid behavior as expected. In these catalysts, segregated phases deposited on the surface were observed and most probably they inhibit the catalytic properties of the spinel.

4. Conclusions

α-Fe_2O_3 and ZnO are segregated from the spinel $ZnFe_{2-x}Al_xO_4$ compound if aluminum content is high; crystallite size decreases with increasing aluminum content, and the lattice parameters for catalysts with a high aluminum content deviate from Végard's law prediction.

A decrease in the symmetry of the electric field gradient at Fe^{3+} nucleus is observed as the x value increases. This result may be associated to the spatial accommodation of Al cations in the octahedral sites in the spinel structure, which gives rise to a charge transfer from iron to oxygen in the Fe–O bond. Hence, oxygen atoms turn out to be more basic and the acid–base type dissociation during the 1-butene activation is favored. Therefore, the dilution of the active sites on the oxidative dehydrogenation of 1-butene to butadiene is not observed.

From the results presented in our previous paper [7] and the present study, catalysts with a high content of iron in the mixed oxides (Zn, Fe, Al)–O favor the oxidative dehydrogenation of 1-butene. The substitution of iron by aluminum (in the octahedral sites of the spinel) increases the efficiency of the catalyst for the oxidative dehydrogenation, such as in the conventionally used catalysts [5] (Zn, Fe, Cr)–O. Therefore, interactions between Cr and Fe or Al and Fe generate similar active sites on the spinel surface.

As the iron content is related to the active sites, the higher the amount of iron, the higher is the selectivity; furthermore, selectivity is independent of the Fe^{3+} interaction with the spinel. However the same trend is not observed for activity. In our previous work for low iron content it was found that catalytic activity increased with iron content. In this work, for high iron contents it is concluded that activity decreases as iron content increases. An optimum composition is found: for $x \approx 1.0 = Al/Fe$ ratio. Hence, a spinel intermediate structure favors activity and selectivity. The α-Fe_2O_3 is not selective, the $ZnFe_2O_4$ or $ZnAl_2O_4$ activities are low.

References

[1] H. Wise, J. Oudar, Material Concepts in Surface Reactivity and Catalysis, Academic Press, 1990, p. 135.
[2] D.L. Trimm, Design of Industrial Catalysts, Elsevier, 1980, p. 137.
[3] V.D. Sokolovskii, Catal. Rev. Sci. 32 (1990) 1.
[4] Y.D.S. Cheng, S.B. Lee, Appl. Catal. 70 (1991) 161.
[5] R.J. Rennard, W.L. Kelh, J. Catal. 21 (1971) 282.
[6] H. Armendariz, J.A. Toledo, G. Aguilar-Ríos, M.A. Valenzuela, P. Salas, A. Cabral, H. Jiménez, I. Schifter, J. Mol. Catal. 92 (1994) 325.
[7] J.A. Toledo, M.A. Valenzuela, H. Armendariz, G. Aguilar-Ríos, B. Zapata, A. Montoya, N. Nava, I. Schifter, Catal. Lett. 30 (1995) 279.
[8] T. Simons, E. Verheijen, P. Batist, G. Schuit, Adv. Chem. Ser. 76 (1968) 271.
[9] B.L. Yang, F. Hong, H.H. Kung, J. Phys. Chem. 88 (1984) 2531.
[10] B.L. Yang, M.C. Kung, H.H. Kung, J. Catal. 69 (1984) 506.
[11] L.J. Alvarez, J.E. Sánchez-Sánchez, J. Fernández Sanz, J.A. Odriozola, 3rd UNAM-CRAY Supercomputing Conference, August 12–16, 1996, Cambridge University Press, in press.
[12] J.P. Jacobs, A. Malta, J.G.H. Reintjes, J. Drimal, V. Ponec, H.H. Brongersma, J. Catal. 147 (1994) 294.

[13] K.T. Nguyen, H.H. Kung, J. Catal. 122 (1990) 415.
[14] Z.R. Ismagilov, S.N. Pak, V.K. Yermolaev, J. Catal. 136 (1992) 197.
[15] L.V. Azaroff, Elements of X-Ray Crystallography, McGraw Hill, London, 1968, p. 552.
[16] H.P. Klug, L.E. Alexander, X-ray Diffraction Procedures, Wiley, New York, NY, 1974, p. 562.
[17] D.R. Lide, Handbook of Chemistry and Physics, CRC Press, Boca Raton, FL, 71st ed., 1990–1991, p. 12-1.
[18] J.A. Dumesic, H. Topsøe, Adv. Catal. 26 (1977) 121.
[19] M.D. Osborne, M.E. Fleet, G.M. Bancroft, J. Solid State Chem. 53 (1984) 174.
[20] H.M. Gager, M.C. Hobson, Catal. Rev. Sci. Eng. 11 (1975) 1.
[21] A.Z. Hrynkiewicz, A.J. Pustowka, B.D. Sawicka, J.A. Sawicki, Phys. Status Solidi (a) 9 (1972) 607.
[22] W. Künding, K.J. Ando, R.H. Lindquist, G. Constabaris, J. Phys. B 17 (1967) 467.
[23] R.W. Cares, J.W. Hightower, J. Catal. 23 (1971) 193.
[24] D.J. Hucknall, Selective Oxidation of Hydrocarbons, Academic Press, New York, NY, 1974, p. 75.
[25] K. Tanabe, M. Misono, Y. Ono, H. Hottori, Stud. Surf. Sci. Catal. 51 (1989) 215.